JOURNAL OF AUTOMOTIVE POWERTRAIN AND TRANSPORTATION TECHNOLOGY
e-ISSN: 2821-286X

JAPTT

Vol. 4 No. 1 (2024) 8-17
https://publisher.uthm.edu.my/ojs/index.php/japtt

CFD Analysis on the Aerodynamic Characteristic of Medium Sized-Car Vehicle Moving Under the Influence of Steady Crosswind

Muhammad Hamizan Noor[1], Izuan Amin Ishak[1]*

[1] *Department of Mechanical Engineering Technology, Faculty of Engineering Technology, Universiti Tun Hussein Onn Malaysia, 84600 Panchor, Pagoh, Johor, MALAYSIA*

*Corresponding Author: izuan@uthm.edu.my
DOI: https://doi.org/10.30880/japtt.2024.04.01.002

Article Info

Received: 20 April 2024
Accepted: 5 November 2024
Available online: 30 December 2024

Keywords

Aerodynamics, car vehicle, flow structure, steady crosswind

Abstract

Vehicle aerodynamics is a critical issue to investigate, particularly for those concerned with safety criteria. For instance, the issue of crosswind effect on a moving car vehicle is an example of a critical road safety driving situation. In this article, Computational Fluid Dynamics (CFD) analysis is carried out using ANSYS Fluent software to investigate the influence of crosswind on a moving car vehicle. The car model used in this study will be a medium-sized vehicle from the C-segment (i.e. the sedan car). The manipulating variables in this study will be the yaw angle (i.e. the different crosswind conditions) which are 0°, 15°, 30°, 45°, 60°, 75° and 90° and different of inlet velocity 10m/s and 30 m/s. The analysis of the aerodynamic loads (i.e. side force, lift force and drag force) and associated flow structures is carried out to measure the aerodynamic behaviours when the car is moving under different crosswind conditions. From the result obtained, it shows that the different yaw angles affect the aerodynamic performance and the stability of the vehicle itself. However, the effect of different vehicle speeds is not many changes in terms of aerodynamic loads. When the yaw angle increased, the side force is also increased, and the stability of the car is decreased. Conclusively, the highest side force occurs when the yaw angle is at 90°. In terms of the flow structures, because of the flow separation, the high-pressure region gradually migrated more to the windward area and the low-pressure region shifted to the leeward area and the top of the vehicles as the yaw angle grew.

1. Introduction

Nowadays, cars vehicle is very important, especially in transportation. Automobile manufacturers build vehicles to achieve superior fuel efficiency, safety, and stability, even at higher vehicle speeds [1]. A trend in passenger car development is towards larger interiors to improve driver and passenger comfort. This invariably affects the outer form and enhances the effect of aerodynamic forces. Since crosswind stability is a safety concern, thorough information regarding the physics of flow behaviour around the vehicle in a crosswind is desirable. To assess a car vehicle's crosswind stability, numerous investigations must be conducted [2]. The primary aerodynamic loads to consider while analysing the car lateral stability (overturning or rollover) in crosswinds are the side force, lift force, and the rolling moment [3]. When the wind comes from the side, the flow field around the cars becomes asymmetrical, resulting in lateral forces and a yawing moment. In the recent decade, our country Malaysia had a serious problem with a traffic accident. The rise in road accidents in Malaysia is linked to the country's fast

demographic, economic, industrialization, and motorization industries [4]. There are a few cases reported that happened due to the crosswind. Strong winds affect road travel by causing reduced speed limits or even road closures. For an instant suggested a degree of danger index based on the calculation of vehicle lateral deviation from the driving line within the first 0.8 seconds after the wind starts to blow [5]. Next according to Baker, crosswind incidents can be divided into three categories rollover accidents, sideslip accidents, and rotating accidents [5]. Hucho and Sovran, point out that the behaviour of a vehicle in a crosswind is primarily determined by two factors which are the side force and the yawing moment [3].

Computational Fluid Dynamics (CFD) systems use numerical methods and equations to solve fluid flow issues, particularly in the context of vehicle aerodynamics [6]. CFD aids in the prediction of fluid flow dynamics utilising software tools and mathematical modelling. It is currently widely utilised and accepted in the industry as a viable engineering tool [7]. Three separate CFD approaches are used to simulate airflow and aerodynamics which are Reynolds-Averaged Navier-Stokes (RANS), unstable RANS (URANS), and Large Eddy Simulation (LES) [6]. According to the research, the Reynolds-Averaged Navier-Stokes (RANS) technique is the most commonly used CFD technique because of its low computing cost and ability to produce accurate and trustworthy simulation results. Various turbulence models are available in the Reynolds-Averaged Navier-Stokes (RANS) approach, including Standard $k-\varepsilon$ that are uses in this study. The evaluation of fluid flow under its physical parameters such as velocity, pressure, temperature, density, and viscosity are accomplished in an extremely CFD software analysis. By using the CFD, a considerable understanding of the fundamental flow characteristics is achievable, since the evaluation process can be considered more efficient and less expensive [8].

Aerodynamics is the study of forces and the resulting motion of objects through the air. The aerodynamic characteristics are determined by the body shape of the vehicle. One of the most significant factors influencing a car's dynamic performance is aerodynamics [9]. For an instant, the response to crosswinds is an important aspect of aerodynamic stability [10]. In general, aerodynamic configuration reduces air turbulence and drag [11]. The major responsibility of the passenger car aerodynamicist is to provide acceptable high-speed stability while ensuring competitive aerodynamic drag [10]. The largest influence will come from the powertrain, but both aerodynamic drag and weight reduction will be required, and both trends are projected to increase. If significant weight reduction is possible, it will have ramifications for aerodynamic development, as providing acceptable aerodynamic stability becomes more difficult [10].

Aerodynamic forces and moments are made up of three vertical forces and torques along the -x, y, and z axes, also known as six aerodynamic component forces. These forces include the drag force, lift force, side force, rolling moment, pitching moment, and the yawing moment [12]. The drag force is the force exerted by oncoming air on a moving body. It's the resistance that the air provides to body movement. As a result, when a vehicle moves, it displaces the air. Hence, affect the car's speed and performance is highly affected due to drag. Secondly, the force that opposes the car's weight and keeps it on the ground is known as lift. Any part of the car generates lift, but the shape of the car body generates the majority of it in a regular car. The motion of the car through the air produces lift, which is a mechanical aerodynamic force. Thirdly, side force is the lateral (i.e., parallel to wheel axis) force produced by a vehicle tire during cornering. Tire slip generates cornering power, which is proportional to slip angle at low slip angles. Relaxation duration describes the rate at which cornering force builds up. Side force is also generated once a vehicle moves under crosswind conditions.

The Reynolds number (*Re*) is the ratio of inertial forces to viscous forces. The *Re* is a dimensionless number that is used to classify fluid systems in which the effect of viscosity is essential in regulating fluid velocities or flow patterns. The *Re* is classified mathematically as shown in Eq. 1.

$$Re = \rho \times V \times H \tag{1}$$

where ρ is the density of the fluid, v is the velocity of the fluid, H is the characteristics length of an object, and μ is the dynamic viscosity of the fluid. When determining whether fluid is in laminar or turbulent flow, *Re* the is used. A *Re* less than or equal to 2100 indicates laminar flow, while a *Re* greater than 2100 indicates turbulent flow, according to API 13D guidelines. In the analysis of flow over a vehicle, the usual *Re* used by previous researchers is between 4×10^5 (no crosswind) to 4.5×10^5 (with crosswind condition) [13]. Mostly, the value of Re is dependent on the vehicle speed (i.e. relative velocity of the fluid) and the geometry of the object.

The boundary layer, or flow, starts to separate when the incoming flow hit the body surface. This is referred to as a boundary layer separation or flow separation. The flow separation and reattachment around the car in which has significant effects on the aerodynamics of the vehicle. Because flow is unable to adhere to the vehicle surface, flow separation occurs in the vehicle at the back end. The flow separation occurs because the boundary layer travels far enough against an adverse pressure gradient that the boundary layer's speed relative to the vehicle approaches zero [14]. And the flow separates from the vehicle surface, taking the shape of eddies and vortices, creating a low-pressure area known as the wake region [14].

This paper has been organized in the following way. In Section 2, the model description, the steps involved in the simulation, and the grid-independent test is discussed. Section 3 prevails the result and discussions in terms of aerodynamic loads and the flow structure. Lastly, Section 4 will conclude the article's findings.

2. Methods

2.1 Model Description

The model used in this study is a sedan car model which is the medium size of vehicle that represents a C-segment car. This model is designed by using SOLIDWORKS software by referring to the actual geometry. **Fig. 1** shows the overall view of the car model whilst **Table 1** provides the general dimension of the proposed vehicle.

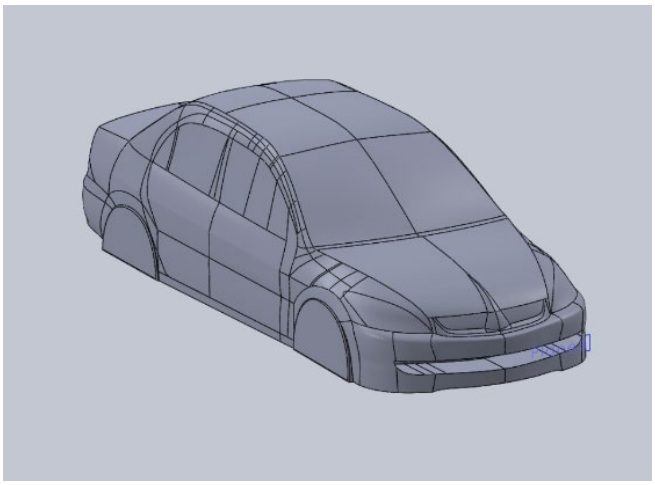

Fig. 1 *CAD model for segment C car*

Table 1 *General dimension of proposed C-segment car*

Dimension of the model	Dimensions (mm)
Length	4506
Width	1690
Height	1392

2.2 Steps in Performing ANSYS Simulation

There are three major steps for performing an ANSYS Fluent simulation which is pre-processing, solving, and post-processing. The creation of a 3D model is the initial stage before starting the simulation. A 3D model is imported from SOLIDWORKS to ANSYS in this project. Before the meshing process begins, the model is created in ANSYS, and the fluid domain is formed. To simulate fluid, analysis tools used fluid domains or enclosures. **Fig. 2** illustrate the enclosure's dimensions, which are H = 1.392 m, L = 1.392 m and ground clearance for this car segment is 0.14 m.

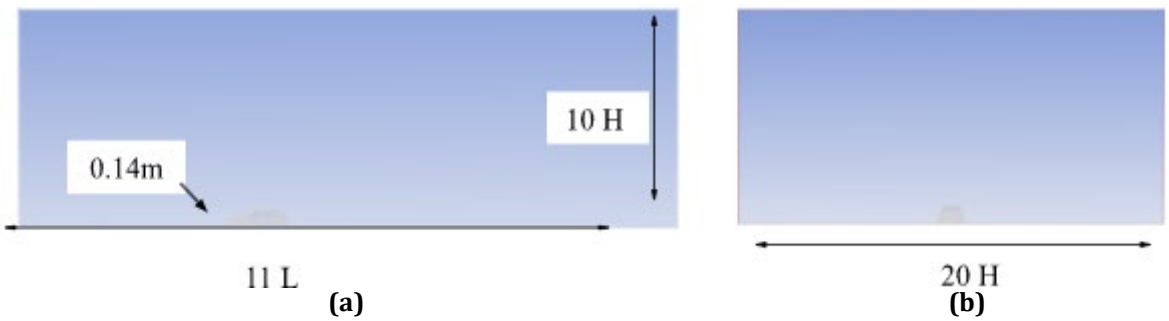

Fig. 2 *(a) Side view of the enclosure; and (b) front view of the enclosure*

After that is the meshing process. The meshing process is one of the most important steps for simulation to produce a good simulation result. The cell mesh model is correlated with the Mechanical Design Model branch in Mechanical Design Analysis Systems or Mechanical Model Component Systems, and it affects the geometry definition, coordinate systems, connections, and generates the model definition mesh branches [14].

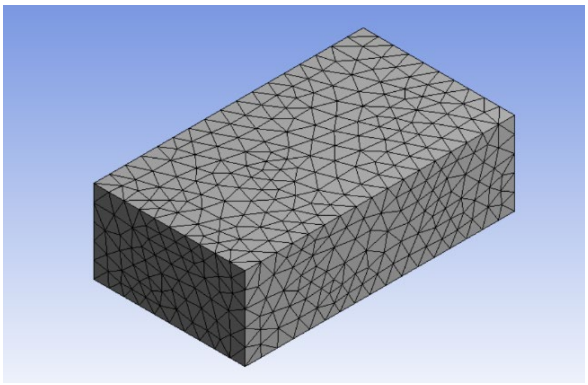

Fig. 3 *Complete mesh of the enclosure*

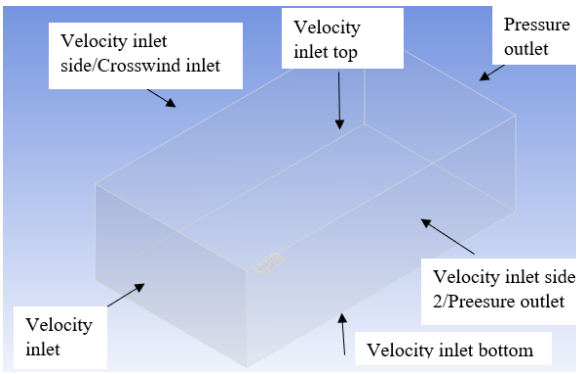

Fig. 4 *Boundary conditions for the enclosure surfaces*

Fig. 3 shows the complete mesh of the enclosure. The meshing procedure, which discretizes the model into numerous elements, comes next. In order for the simulation to give a decent outcome, the meshing technique is critical. The project was made on a triangular mesh. The quality of the findings is determined by the mesh efficiency. During the meshing procedure, the inlet and outlet of the model are described. The total number of meshes in this scenario is 78,821 nodes. To acquire reliable CFD analysis results, a suitable boundary condition must be set **Fig. 4** shows the boundary conditions for the enclosure with no crosswind condition and with crosswind condition. The model's boundary conditions, such as the velocity inlet, pressure outlet, vehicle surface, wall roughness, and flow type, must be defined after the meshing technique is completed. The Reynolds number used in this study are between 4×10^5(no crosswind) to 4.5×10^5 (with crosswind condition) (equivalent to inlet velocity of 30 m/s) as per the validated paper [13].

Table 2 *Boundary conditions*

Detail	Boundary Condition	Value
Inlet	Velocity Inlet/Crosswind Inlet	10 m/s and 30 m/s
Outlet	Pressure Outlet	0 Pa (gauge)
Vehicle surface	Wall Boundary	No-slip wall

2.3 Grid Independence Test

The simulation with no crosswind is chosen to undergo for the grid independence test. As indicated in **Table 3**, seven types of curvature normal angles were generated based on high-quality mesh for further analysis in order to discover the optimal mesh resolutions. Consequently, the numbers of nodes are changed because of the differences in the curvature normal angle. From each of these cases, the value of coefficient of drag (C_d**)** is obtained in order to assess the grid dependency. The velocity inlet used in these simulations is 30 m/s.

Table 3 *Different mesh resolutions based on high-quality mesh and curvature normal angles*

Curvature normal angles	18°	13°	9°	7°	5°	3°	1°
Number of nodes	65,626	69,845	75,238	78,821	83,665	90,951	109,005
Coefficient of drag, C_d	0.2031	0.1977	0.2003	0.1904	0.1913	0.1920	0.1895

Fig. 5 illustrates that the drag coefficient (C_d) is 0.1904 when the number of nodes reaches 78,821 nodes. Following that, the C_d value has no significant changes. As a result, node 78,821 has been chosen as the grid's convergence point, and this setting will be used throughout the study.

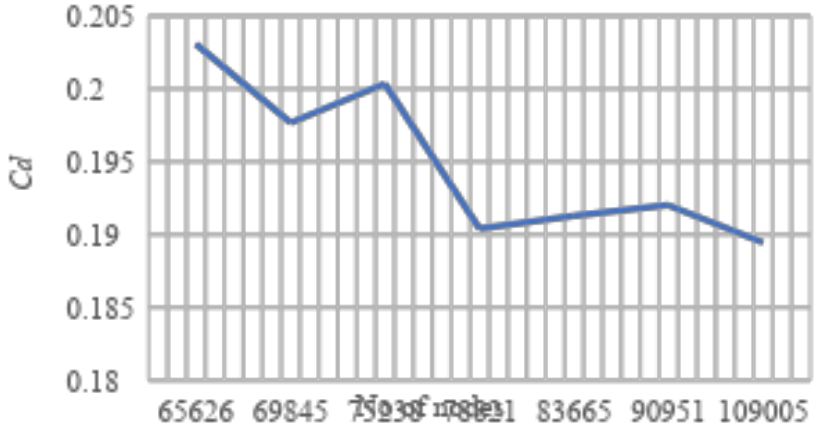

Fig. 5 *Value of C_d based on no crosswind simulation at 30 m/s inlet speed*

Figure 2.5 illustrates that the drag coefficient (C_d) is 0.1904 when the number of nodes reaches 78,821 nodes. Following that, the C_d value has no significant changes. As a result, node 78,821 has been chosen as the grid's convergence point, and this setting will be used throughout the study.

3. Results and Discussion

3.1 Drag Coefficient

Fig. 6 shows the result of the coefficient of drag (C_d), against the difference of yaw angle and velocity inlet. Seven different wind conditions are used in this study which is 0° to 90° with two different inlet speeds which are 30 m/s and 10 m/s which represent the vehicle speed of 108 km/h and 36 km/h. From Figure 3.1 it shows that, as the yaw angle increase from 0° to 15°, the C_d is also increased. Then, it can be seen that when the yaw angle increase from 15° to 30° the C_d is decreased. From 30° to 60° as the yaw angle increases the C_d also increase. Lastly, from wind conditions 60° to 90°, it can be seen that the value of C_d decreased substantially. In general, it can be observed that the value of C_d with the vehicle speed of 30 m/s and 10 m/s is not so much changed in values.

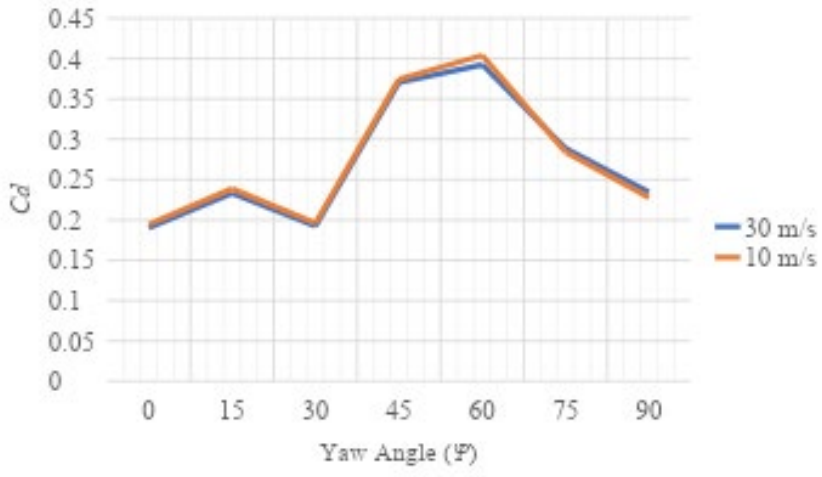

Fig. 6 *Coefficient of drag (C_d) against the difference of yaw angle and velocity inlet*

3.2 Lift Coefficient

Fig. 7 shows the result of the coefficient of lift force (C_l), against the difference of yaw angle and velocity inlet. From the figure, it shows that, as the yaw angle increase from 0° to 15°, the value of C_l is also increased with both

inlet speeds. Then, when the yaw angle increases from 15° to 45°, for the 30 m/s inlet speed, the value of C_l is stagnant horizontally. However, for the 10 m/s inlet speed, from the yaw angle 15 to 30, the value of C_l shows an increasing pattern before becoming stagnant until the yaw angle of 45°. From the wind conditions of 45° to 75°, as the yaw angle increases the C_l also increase. Lastly, from 75° to 90°, it can be visualized that the C_l is decreased. In general, the value of C_l with the vehicle speed 30 m/s and 10 m/s is not so much changed except from the yaw angle 15° to 45°.

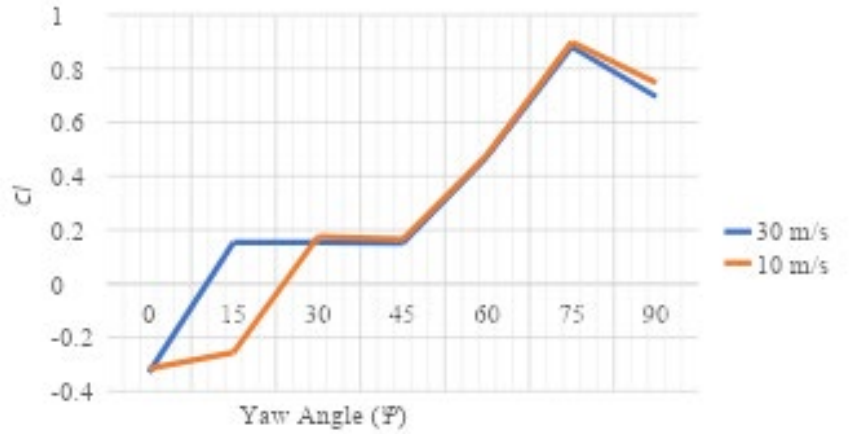

Fig. 7 *Coefficient of lift (C_l) against the difference of yaw angle and velocity inlet*

3.3 Side Coefficient

Fig. 8 shows the result of the coefficient of side (C_s), against the difference of yaw angle and velocity inlet. From the figure, it shows that, as the yaw angle increase from 0° to 90°, the C_s is also increased. This is theoretically accepted as the wind flow is shifted towards the windward side of the car, hence the increase in C_s values. Furthermore, it is obvious to also see that there are no significant differences between different inlet speed cases.

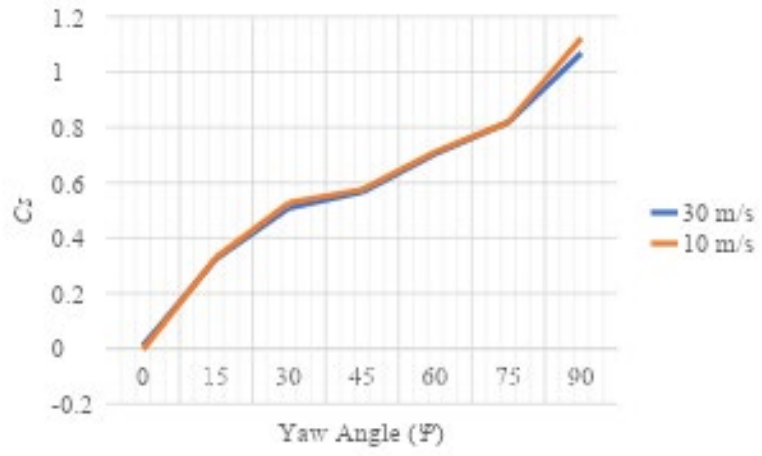

Fig. 8 *Coefficient of side (C_s) against the difference of yaw angle and velocity inlet*

3.4 Flow Structure

For the flow structure, the analysis is presented through the pressure contour and velocity streamline based on one a high Reynolds Number only (i.e. with inlet velocity of 30 m/s). This is because based on the results of aerodynamic load obtained earlier, there are no significant differences in the value of the coefficient of drag, coefficient of lift and coefficient of side recorded.

3.4.1 Pressure Contour on Vehicle Surface

Fig. 9 shows the pressure acting on a different surface of the car body because the crosswind comes in different yaw angle conditions (Ψ). For the 0° of yaw angle or no crosswind, when the flow comes and hits the body, the high pressure is acting on the front bumper of the car because the flow gets hit directly and then the pressure become decrease when it flows to the car hood because the flow separation at right and left. The pressure at the

windshield is quite high because the wind gets hit directly and when it flows to the roof the pressure is low because of the flow separation at the roof and high again when it moves to the back of the hood. The lowest pressure is found at the rear bumper because there is no wind hitting it.

When the yaw angle is increased to 15°, the high pressure shifted to windward and front of the car. At the windshield area, there is a little pressure acting and the pressure is low at the leeward because of the flow separation that happens to the leeward area. Then when the crosswind increased to 30°, 45°, 60° and 75° the same thing happens where the high pressure slowly shifted more to the windward area and low at the leeward area and the top of the car because of the flow separation.

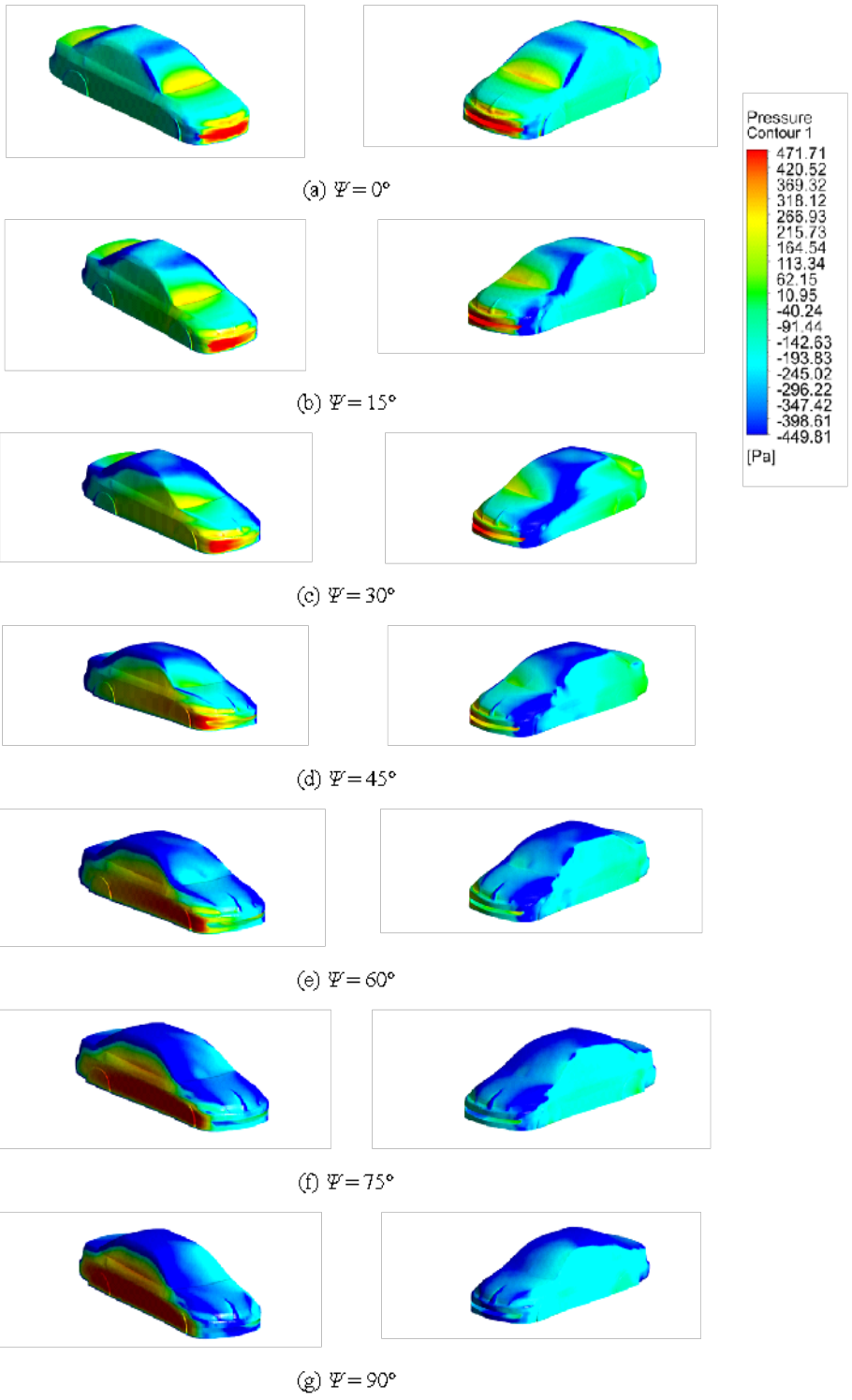

Fig. 9 *Pressure contour on vehicle surface for different crosswind conditions*

When the yaw angle reaches 90°, the high pressure is acting on all windward areas or side areas of the vehicle and the pressure is low at top of the car and leeward area because of the flow separation that happens when it flows to the top of the vehicle. This can be contributed to the Bernoulli principle which stated that a rise in a fluid's speed is accompanied by a drop in static pressure or a decrease in the fluid's potential energy.

3.4.2 Velocity Streamline from Top View

Fig.10 shows the velocity streamlines superimposed on the mean pressure contour from the top view for different crosswind conditions. To disclose the horizontal plane structures of flow over the car, the streamline velocity has been revealed. The streamlines were acquired on a plane placed horizontally across the car which originates from the middle of the car. For the no crosswind condition or 0° yaw angle, there is high pressure in front of the car and low pressure behind the car. The velocity streamlines directly hit the front of the bumper and its flows on the car. There is a slight vortex formed at the back of the car due to the flow separation and reattachment.

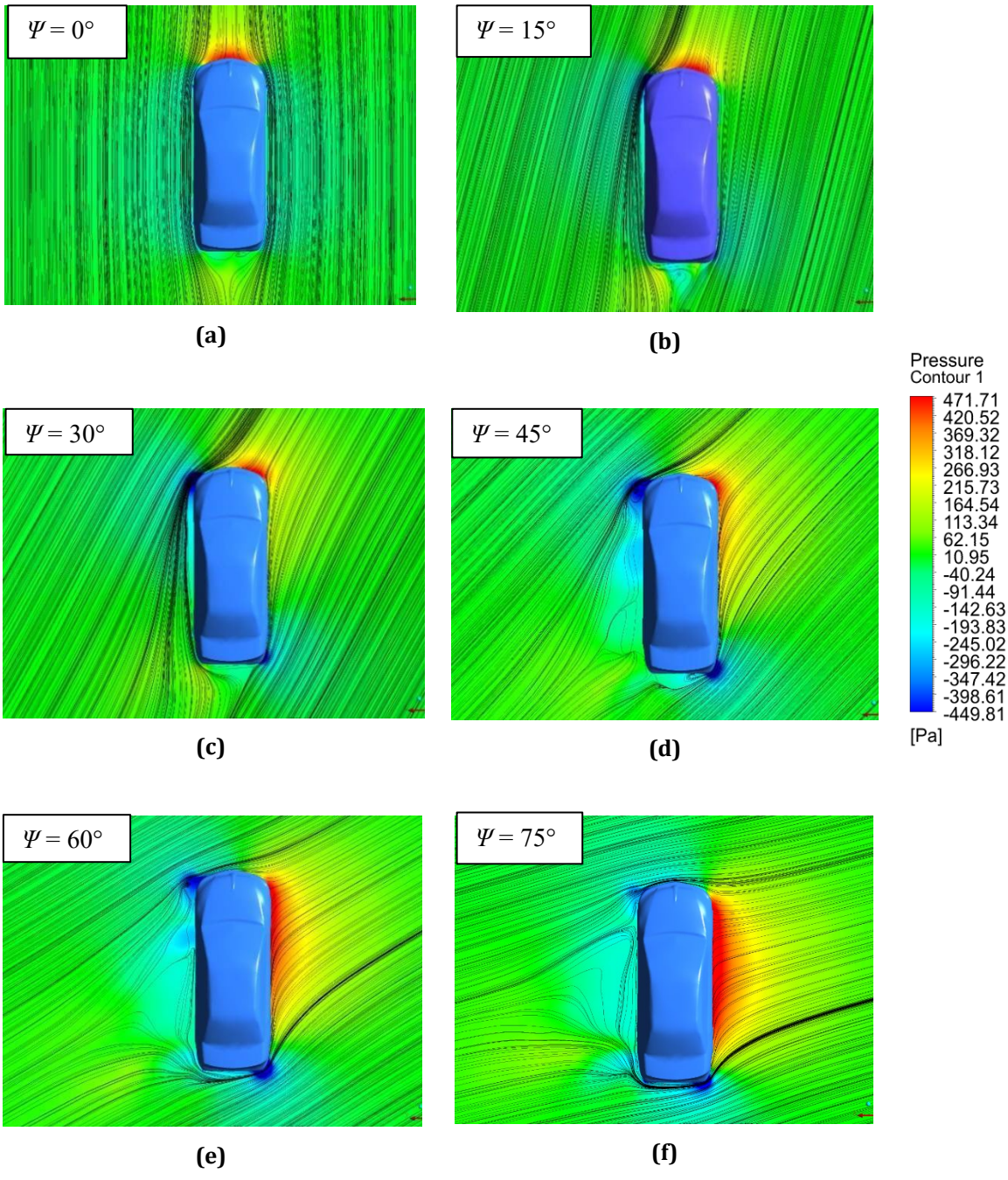

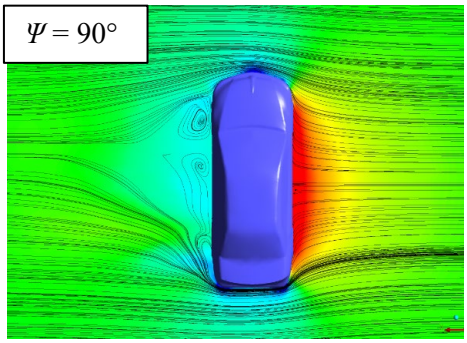

(g)

Fig. 10 *Velocity streamlines superimposed on the mean pressure contour from top view for different crosswind conditions*

When the yaw angle of the crosswind is increased from 0° to 15° the high pressure slowly shifts to the windward area as shown in **Fig. 10**. Then, when the crosswind conditions are increased furthermore to 30°, 45°, 60°, 75° and 90°, the same thing happens which is the high pressure slowly shifted to the windward area. For the 90° yaw angle the high pressure is shifted to all side areas or leeward areas. Thus, it can be concluded that the higher the yaw angles the higher the pressure in the windward area. The result presented here is aligned with Section 3.4.1: Pressure Contour on Vehicle Surface. When the yaw angle increased the vortex also starts to form on the leeward region due to the occurrence of flow separation.

4. Conclusion

The purpose of this research is to see how the influence of the difference crosswind conditions, and Reynolds numbers (i.e. different vehicle speeds) affects the aerodynamic performance of a vehicle. ANSYS CFD software (Fluent) is used to investigate the aerodynamic characteristics on a wide range of crosswind yaw angles conditions. In terms of the key finding related to the stability of crosswind on the vehicle, it can be concluded that the side force coefficient (C_s) is the most important parameter to be taken into account.

From the result attained, the value of C_s rises as the yaw angle of the crosswind rises. Secondly, in terms of different Reynolds numbers used, i.e. when the inlet speed changes from 10 m/s to 30 m/s, there are no significant changes in terms of drag coefficient (C_d), lift coefficient (C_l) or the side coefficient (C_s). In terms of flow structure analysis, it can be observed that the velocity streamlines are hugely affected by the wind conditions. As the yaw angle increases, the vortices formed on the leeward area becomes larger. This happened due to the flow separation that occurs as the flow shifted from 0° to 90°. Last but not least, this aerodynamics study could be extremely beneficial to public and passenger vehicles, particularly in terms of reducing fuel consumption, improving performance, and improving vehicle stability.

Acknowledgement

The authors would like to thank the Faculty of Engineering Technology, Universiti Tun Hussein Onn Malaysia for all the support during project accomplishment.

Conflict of Interest

Authors declare that there is no conflict of interests regarding the publication of the paper.

Author Contribution

The authors confirm contribution to the paper as follows: ***study conception and design****: Muhammad Hamizan Noor;* ***data collection****: Muhammad Hamizan Noor;* ***analysis and interpretation of results****: Muhammad Hamizan Noor and Izuan Amin Ishak;* ***draft manuscript preparation****: Muhammad Hamizan Noor. All authors reviewed the results and approved the final version of the manuscript.*

References

[1] G. Shankar and G. Devaradjane, "Experimental and Computational Analysis on Aerodynamic Behavior of a Car Model with Vortex Generators at Different Yaw Angles," *J. Appl. Fluid Mech.*, vol. 11, no. 1, pp. 285–295, 2018.

[2] I. A. Ishak *et al.*, "Aerodynamic characteristics around a generic train moving on different embankments under the influence of crosswind," *J. Adv. Res. Fluid Mech. Therm. Sci.*, vol. 61, no. 1, pp. 106–128, 2019.

[3] I. A. Ishak, N. Maruai, F. M. Sakri, and R. Mahmudin, "Numerical Analysis on the Crosswind Influence Around a Generic Train Moving on Different Bridge Configurations," vol. 2, no. 2, pp. 76–98, 2022.

[4] M. G. Masuri, K. A. M. Isa, and M. P. M. Tahir, "Children, Youth and Road Environment: Road Traffic Accident," *Procedia - Soc. Behav. Sci.*, vol. 38, no. December 2010, pp. 213–218, 2012, [Online]. Available: http://dx.doi.org/10.1016/j.sbspro.2012.03.342.

[5] M. Batista and M. Perkovič, "A Simple Static Analysis of Moving Road Vehicle Under Crosswind," *J. Wind Eng. Ind. Aerodyn.*, vol. 128, pp. 105–113, 2014.

[6] Muhammad Nabil Farhan Kamal *et al.*, "A Review of Aerodynamics Influence on Various Car Model Geometry through CFD Techniques," *J. Adv. Res. Fluid Mech. Therm. Sci.*, vol. 88, no. 1, pp. 109–125, 2021, doi: 10.37934/arfmts.88.1.109125.

[7] A. N. Nazri, I. A. Ishak, N. Darlis, Z. M. Salleh, and S. F. Zainal, "Aerodynamic Analysis on the Effects of Different Type of Train' s Nose Design u sing Ansys Software," vol. 2, no. 1, pp. 1–9, 2020.

[8] B. Zala, P. P. Rathod, and S. S. Arvind, "Aerodynamic Performance Assessment of Sedan and Hatchback Car by Experimental Method and Simulation By Computational Fluid Dynamics-," *J. Eng. Res. Stud.*, vol. III, no. 1, pp. 91–95, 2012.

[9] J. Wang, H. Li, Y. Liu, T. Liu, and H. Gao, "Aerodynamic Research of a Racing Car Based on Wind Tunnel Test and Computational Fluid Dynamics," *MATEC Web Conf.*, vol. 153, pp. 1–5, 2018.

[10] J. Howell, K. Garry, and J. Holt, "The Aerodynamics of a Small Car Overtaking a Truck," *SAE Int. J. Passeng. Cars - Mech. Syst.*, vol. 7, no. 2, pp. 626–638, 2014.

[11] A. R. Norwazan, A. J. Khalid, A. K. Zulkiffli, O. Nadia, and M. N. Fuad, "Experimental and Numerical Analysis of Lift and Drag Force of Sedan Car Spoiler," *Appl. Mech. Mater.*, vol. 165, pp. 43–47, 2012, doi: 10.4028/www.scientific.net/AMM.165.43.

[12] "A Study on the Segmentation of Korea Insurance Industry Index," 금융공학연구, vol. 19, no. 4, pp. 171–193, 2020.

[13] T. Y. K. and S. H. LEE, "Effect of Crosswind on the Aerodynamics of Two Passenger Cars Crossing Each Other," Int. J. …, vol. 13, no. 2, pp. 293–300, 2012, [Online]. Available: http://link.springer.com/article/10.1007/s12239-012-0027-2.

[14] A. Ahmed, J. I. Siddique, and M. Sagheer, "Dual Solutions in a Boundary Layer Flow of a Power Law Fluid Over a Moving Permeable Flat Plate with Thermal Radiation, Viscous Dissipation and Heat Generation/Absorption," Fluids, vol. 3, no. 1, pp. 1–16, 2018.